Surface Plasmons and Visible Light Iniferter Initiated Polymerization for Nanolocal Functionalization of Mesoporous Separation Layers

Daniel John, Mathias Stanzel, and Annette Andrieu-Brunsen*

Although the technological relevance of mesoporous ceramic polymer hybrid materials is well accepted, missing functionalization concepts enabling 3D nanoscale local control of polymer placement into mesoporous materials, including thin films, and ideally using controlled polymerization techniques limit the application potential. Here, nanolocal functionalization of mesoporous separation layers using controlled, visible light iniferter initiated polymerization allowing responsive polymer functionalization locally limited to the irradiated spot is introduced. Thereby, two visible light sensitive iniferters, s-p-trimethoxysilylbenzyl-S´-dodecyltrithiocarbonate and 4-cyano-4-((dodecylsulfanylthiocarbonyl)sulfanyl)pentanoic acid, are developed for polymer functionalization of mesoporous films in a grafting from and a grafting through approach. 3D nanolocal polymer placement close to the proximity of the plasmonic field source is demonstrated by combining these visible light iniferter initiated polymerizations with optical near field modes, such as localized surface plasmon resonance (LSPR). As the location of the LSPR in mesoporous films can be controlled by placing metal alloy nanoparticles into these films and film thicknesses can be adjusted, this strategy is applied for precise positioning of polymers into mesoporous films with nanolocal control in three dimensions and thus reduces the gap in precision of functional group positioning between technological and biological nanopores.

1. Introduction

Mesoporous oxide films are materials with technological relevance in sensing,[1] molecular sieving,[2] catalysis, and energy conversion.[3] All these technologies depend on molecular transport in nanoscale pores. Often inspired by the structural precision and performance of biological pores, transport through mesopores has been strongly investigated within the last two decades and especially polymers have been used to implement new functions and specific transport characteristics into such nanoscale pores. In this context, polymer functionalization of mesopores advanced significantly within the last years. The majority of polymer functionalized mesopores focuses on responsive polymer grafting resulting, for example, in tuneable gating of ionic permselectivity. Within the last decade, gating of mesopore transport has been demonstrated by applying different stimuli such as pH,[4] temperature,[5] presence of ions,[6] light,[7] or voltage.[8] Contemporary studies related to polymer functionalized mesopores demonstrated control of polymer amount and thus controllable functional density in mesoporous silica.[4,9] In addition, our research group recently demonstrated re-initiation of iniferter initiated polymerization resulting in block-*co*-oligomer functionalized silica mesopores.[10] This allows investigation of the influence of chain architecture on mesopore transport and demonstrates the utility of living polymerizations in mesoporous materials to generate multifunctional and multiresponsive pores.[10b,11]

Being inspired by biological pores and their transport performance, their precise local arrangement of functional units within a pore is of interest for transport design. Strategies to locally control the polymer grafting at the nanoscale and especially within mesoporous films are still very limited and have rarely been combined with living polymerization techniques. To date, (nano)local resolution in pore functionalization has been demonstrated by stepwise and thus layer-wise material deposition which could be followed by locally limited polymerization.[12] Very recently, we demonstrated precise placement of three different functional units of molecular and polymeric nature into inverse opal monolayers as model system using orthogonal surface chemistry and wetting control.[13] These approaches result in local functionalization along the porous film thickness, but no simultaneous nanoscale local resolution within x- and y-direction was achieved. In this context, near field mode induced polymerization is a promising approach as the electromagnetic field is localized into nanoscale dimensions. As demonstrated by Soppera and coworkers and by Kreiter and coworkers, near field mode induced chemistry allows nanolocally limited (polymer) functionalization of plasmonic metal nanostructures.[14] Although, tunable by particle size

D. John, M. Stanzel, Prof. A. Andrieu-Brunsen
Ernst-Berl-Institut für Technische und Makromolekulare Chemie
Technische Universität Darmstadt
Alarich-Weiss-Straße 8, Darmstadt 64287, Germany
E-mail: andrieu-brunsen@smartmem.tu-darmstadt.de

The ORCID identification number(s) for the author(s) of this article can be found under https://doi.org/10.1002/adfm.202009732.

**ADVANCED
SCIENCE NEWS**
www.advancedsciencenews.com

**ADVANCED
FUNCTIONAL
MATERIALS**
www.afm-journal.de

and composition of colloidal metal, near field modes, such as surface plasmons, usually emit light in the visible wavelength range larger than 400 nm. Thus, near field mode compatible photopolymerizations have to be selected or developed.

The combination of metal nanoparticles and mesoporous oxide thin films has been demonstrated in several studies in the last 15 years, and such composite materials are proposed for applications in catalysis,[3a,15] optics,[16] and sensing.[17] The bases for this application potential are new properties, which arise due to the synergy of the individual components. Several approaches for incorporation of the metallic nanoparticles into the mesoporous oxide thin films are known and the position inside the porous matrix can be precisely adjusted.[18] Nonetheless, incorporated in the mesoporous matrix, metallic nanoparticles remain accessible for chemical reactions. For example, Angelomé et al. demonstrated the growing and branching of gold nanoparticles that had been immobilized on a glass surface and covered with a mesoporous silica thin film.[19] Furthermore, these systems can be very diverse, as the properties of metallic nanoparticles can be tuned beforehand by following well known synthesis protocols,[20] and mesoporous oxide films are tunable in pore size, film thickness, as well as surface functionalization.[21]

Within the last years, visible light induction has been demonstrated for many polymerization mechanisms such as atom radical transfer polymerization (ATRP),[22] ring opening metathesis polymerization,[23] dye sensitized polymerizations,[14a,24] and iniferter initiated polymerizations.[25] The majority of these visible light induced polymerizations is using wavelengths around 400 nm, which is mostly not suitable for surface plasmon generation. Nevertheless, the number of photopolymerizations induced by larger wavelengths increases. For example, the induction wavelength of ATRP has been shifted to 464 nm by Zhu and coworkers[26] using [Ir(ppy)₃] as photoredox catalyst and to 400–500 nm by Yagci and coworkers[27] performing a metal-free ATRP by using perylene. Only a few examples for polymerizations at higher wavelengths are known and limited to photoinduced electron transfer reversible addition fragmentation termination (PET-RAFT)[28] or dye sensitized polymerizations.[29] Surface plasmon induced polymerizations at wavelength higher than 400 nm have been mainly combined with dye sensitized polymerizations[14a,24] and reversible addition fragmentation termination (RAFT) polymerization using azobisisobutyronitrile (AIBN) as an initiator.[30] Very recently, a first example of so-called plasmon catalyzed PET-RAFT polymerization on gold gratings has been reported.[31] In terms of RAFT polymerizations, a tolerance versus oxygen has been achieved in combination with photoredox catalysts[32] or dyes, for example, Eosin Y, and ascorbic acid.[33] The combination with dyes is even more beneficial, as light above 516 nm becomes suitable for polymerization induction. Furthermore, the catalytic presence of Eosin Y leads to faster reaction kinetics compared to polymerizations in absence of the dye.[34] Furthermore, a PET-RAFT approach, which utilizes zinc tetraphenylporphyrin enabling visible light induction, was very recently applied on planar surfaces by the group of Boyer.[35]

Although, the number of visible light induced controlled or living polymerizations is increasing rapidly at the moment, almost all present studies related to near field induced polymerizations use free-radical polymerization approaches mostly using commercial components which strongly limits their diversity. Thereby, controlled polymerization techniques are of special interest as these would not only allow a certain control on polymer amount, but further provide access to chain composition control in addition to nanolocal placement. However, as the LSPR is usually generated upon visible light irradiation, suitable polymerization techniques are required.

In this context, the first example of nanoscale polymer functionalization using a controlled polymerization reaction has very recently been reported by Soppera and coworkers demonstrating re-initiation using near-field mode induced ATRP, and by this, showing preparation of multifunctional metal/polymer nanostructures.[36] Compared to ATRP, iniferter initiated polymerization is versatile as it offers polymerization control without requiring additional radical sources such as AIBN.[25b,37] This is especially useful for functionalization of nanoscale pores with restricted pore accessibility. The development of such visible light sensitive iniferter molecules attained constantly increasing attraction since 2015,[38] and iniferter polymerization induced by visible light was demonstrated for the first time by the group of Qiao in 2015.[25a]

Here, we demonstrate visible light induced and nanolocal polymer functionalization of mesoporous separation layers using visible light and plasmon induced iniferter initiated polymerization. Therefore, gold-silver alloy nanoparticles (Au/Ag-NPs) were integrated into mesoporous silica films as surface plasmon and thus nanoscale light source. S-p-trimethoxysilylbenzyl-S'-dodecyltrithiocarbonate (SBDTTC) which possesses an absorption maximum at 434 nm in DMSO (Figure S8, Supporting Information) is used to functionalize mesoporous films in a grafting from approach. The iniferter 4-cyano-4-((dodecylsulfanylthiocarbonyl)sulfanyl)pentanoic acid (CDTPA) possessing an absorption maximum at 448 nm in ethanol (Figure S8, Supporting Information) is used to functionalize mesoporous silica films with grafted allyl triethoxysilane (allyl functionalized silica) in a grafting through approach applying visible light irradiation and surface plasmon near field modes of the embedded nanoparticles. Nanolocally limited polymer functionalization is demonstrated for CDTPA by electron microscopy.

2. Results and Discussion

Polymer functionalization of mesoporous thin films is achieved by applying visible light and iniferter initiated polymerization. The iniferter CDTPA is used in a grafting through approach, whereas SBDTTC (synthesis described in the supporting information and characterization shown in Figures S1–S3, Supporting Information) is used in a grafting from approach (**Figure 1**). The polymer placement in mesoporous films is investigated. Dimethylaminoethyl methacrylate (DMAEMA) was used as monomer due to its responsivity to pH and reported transport regulation.[11]

Polymerizations were conducted under visible light irradiation without additional radical sources or catalysts in 600–800 nm thick mesoporous silica films with pore sizes of 12 nm (neck) and 16 nm (Figure S4, Supporting Information).
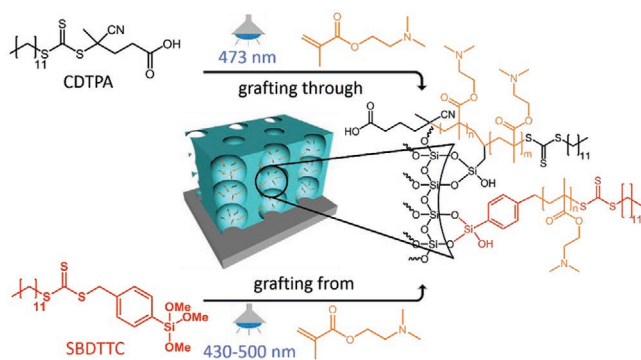
Figure 1. Chemical structures of CDTPA (black) and SBDTTC (red). Polymer functionalization of mesoporous silica films using CDTPA follows a grafting through approach after covalent grafting of allyltriethoxysilane to the mesopore wall, whereas polymer functionalization using SBDTTC is achieved by grafting from after binding SBDTTC to the mesopore wall.

The mesoporous films show a porosity of 55 vol% as calculated by the Bruggeman effective medium theory (BEMT) applying the refractive index determined by ellipsometry at a relative humidity of 20% as further described in literature (see also Table S1, Supporting Information).[10a,39] In order to achieve polymer functionalization in a grafting from approach, SBDTTC is covalently grafted to the mesoporous silica surface. Prior to polymerization under visible light irradiation, the SBDTTC functionalized mesoporous silica films are CO_2-plasma treated for removal of SBDTTC at the outer planar mesoporous film surface according to a protocol from Babu et al.[40] Consequently, polymerization can only proceed within the mesoporous film, but not on the planar outer surface.

The SBDTTC functionalization becomes evident by the mass loss of 20% in TGA-measurements (**Figure 2**c, black and red). The SBDTTC functionalized mesoporous films are then used for visible light induced polymerization. As SBDTTC did not initiate polymerizations under thermal treatment up to 70 °C under the applied experimental conditions (Figures S10–S12, Supporting Information), the increasing C=O stretching vibrational band at 1728 cm^{-1} is attributed to poly(2-(dimethylamino) ethyl methacrylate) (PDMAEMA). Increasing PDMAEMA amount with increasing polymerization time is observed (Figure 2b,c). After 5 h of polymerization, a relative C=O vibrational band intensity of 0.05 at 1728 cm^{-1} (Figure 2b, blue) is observed. By increasing the polymerization time to 17 h, this relative C=O stretching vibrational band intensity at 1728 cm^{-1} increases to 0.08 (Figure 2b, dark yellow). Characterization by TGA shows an initial mass loss of 3% between 100 and 200 °C which is attributed to adsorbed water (Figure 2c, black). The observed mass loss of 7% between 400 and 600 °C is ascribed to chemisorbed water (Figure 2c, black).[41] A total mass loss of 20% at 600 °C is observed for SBDTTC functionalized mesoporous silica films (Figure 2c, red) indicating successful functionalization with SBDTTC. Considering a specific surface area range of 170–610 m^2 g^{-1}, as determined by two different approaches, a grafting density of SBDTTC of 0.44 – 1.59 molecules nm^{-2} is calculated. The upper value is very probably higher than the actual iniferter density, because the specific surface area is rather underestimated due to the sample preparation of scratching off 600–800 nm thick films from a substrate. This is supported by nitrogen sorption of additionally prepared bulk mesoporous silica using the sol in a petri dish under otherwise identical evaporation and calcination conditions resulting in a
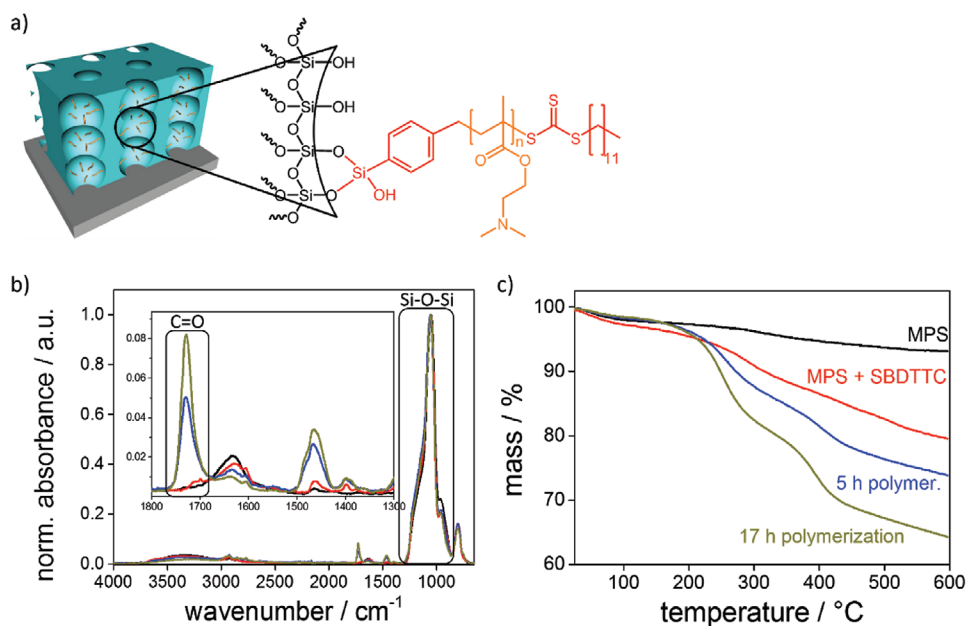

Figure 2. a) PDMAEMA functionalization of CO_2-plasma treated mesoporous silica films in a grafting from approach with surface bound SBDTTC. b) ATR-IR spectra of mesoporous silica (black), mesoporous silica functionalized with SBDTTC (red), after 5 h of polymerization (blue), and after 17 h of polymerization (dark yellow) of DMAEMA on CO_2-plasma treated mesoporous films. For measuring ATR-IR, the films were scratched off the substrate. c) TGA measurements of mesoporous silica (black), mesoporous silica functionalized with SBDTTC (red), and after 5 h (blue) as well as after 17 h (dark yellow) polymerization time of DMAEMA on CO_2-plasma treated mesoporous silica films. Spectra were recorded in air.

**ADVANCED
SCIENCE NEWS**
www.advancedsciencenews.com

**ADVANCED
FUNCTIONAL
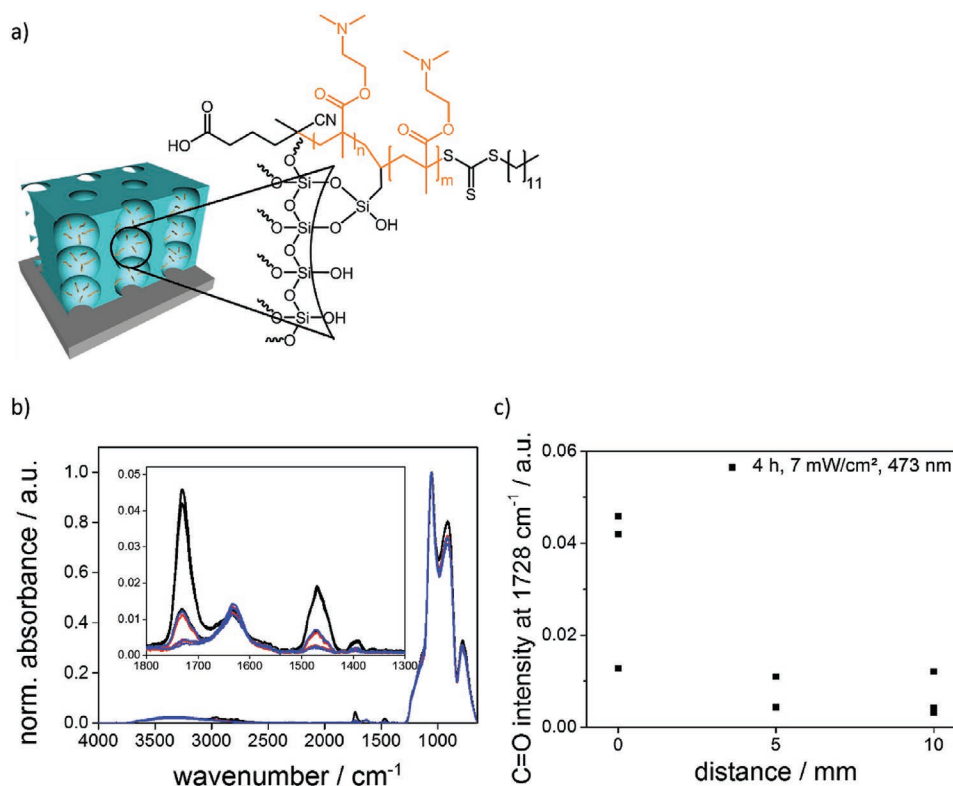MATERIALS**
www.afm-journal.de

Figure 3. a) Schematic representation of PDMAEMA functionalization of allyltriethoxysilane functionalized mesoporous silica films using CDTPA in a grafting through approach. b) ATR-IR spectra recorded after CDTPA induced polymerization of DMAEMA in allyltriethoxysilane functionalized mesoporous silica films under irradiation with a blue laser (473 nm) for 4 h at the laser spot (black spectra), 5 mm distance (red spectra), and 10 mm distance to the laser spot (blue spectra). The ATR-IR spectra of the functionalized mesoporous silica film were recorded directly on the substrate. c) C=O vibrational stretching absorbance at 1728 cm^{-1} normalized to the Si-O-Si vibrational band at 1050 cm^{-1} versus the distance from the laser focused spot recorded at allyl functionalized mesoporous silica films. The polymerizations are carried out in ethanolic solution of DMAEMA (1.7 м) and CDTPA, induced by laser light (473 nm, 7 mW) for 4 h. The irradiation is conducted on 3 individual substrates and the substrates are characterized by ATR-IR spectroscopy at the laser spot, in 5 mm distance, and in 10 mm distance to the laser spot.

surface area of 610 m^2 g^{-1} (Figure S5, Supporting Information). In addition, the anchor group containing three methoxy groups is expected to form multilayers as well reducing the real grafting density as compared to the value of 1.59 molecules nm^{-2}. After an irradiation time of 5 h, a total mass loss of 26% (Figure 2c, blue) is observed, which is correlated to 1 to 2 repeating units of PDMAEMA assuming all iniferter molecules reacted and exhibit identical chain length. In accordance with attenuated total reflexion-infrared (ATR-IR) results, this total mass loss increases to 35% correlating to 4 to 5 repeating units after 17 h irradiation (Figure 2c, dark yellow). As discussed above, the real polymer chain length is expected to be higher as the density of reactive iniferters is expected to be overestimated. Nevertheless, this estimation gives a good idea on the minimum polymer chain length and the maximum chain density within the mesopores. Furthermore, polymer functionalized mesoporous silica films show a typical two step degradation in TGA measurements between 200 and 450 °C which is a clear indication for successful PDMAEMA functionalization of the mesoporous films.[42]

To achieve polymer functionalization in a grafting through approach applying CDTPA, the polymerizable group allyl triethoxysilane is covalently attached to the mesoporous silica surface. As CDTPA shows sufficient absorption at 473 nm (Figure S8,

Supporting Information), irradiation using a 473 nm laser (Figure S13, Supporting Information) results in PDMAEMA grafting as indicated by the C=O stretching vibrational band intensity at 1728 cm^{-1} within the normalized ATR-IR spectra (**Figure 3**).

In addition, the PDMAEMA functionalization can be limited to the laser spot region (Figure 3b black and Figure 3c at 0 mm). In that case, no significant PDMAEMA formation is observed in 5 or 10 mm distance from the laser irradiated spot (Figure 3c) indicating the potential of the applied functionalization concept for locally limited functionalization.

To demonstrate nanolocally limited functionalization of mesoporous silica films applying visible light induced iniferter initiated polymerizations, mesoporous silica films were equipped with Au/Ag-NPs as plasmonic near field source with a suitable wavelength for iniferter initiated polymerization. For this, mesoporous architectures, particularly mesoporous silica double layer and mesoporous allyl silica double layer films with precisely positioned Au/Ag-NPs (**Figure 4**) between the two layers are constructed. In the first step, mesostructured films, silica or allyl silica (co-condensed), were deposited on substrates via dip coating using the well-established EISA process.[43] By amine modification of the outer silica surface via 3-(ethoxydimethylsilyl)propylamine grafting, immobilization
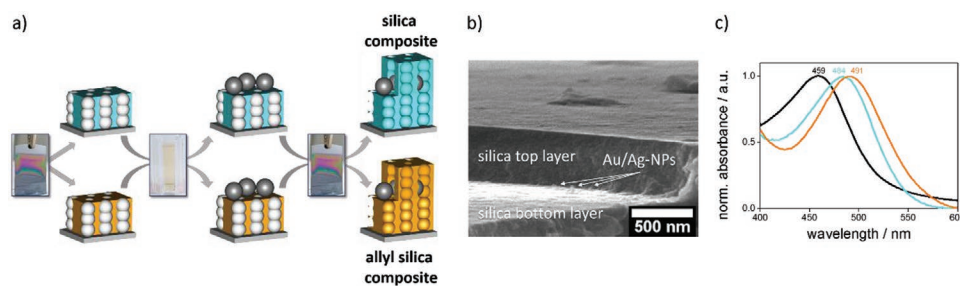
Figure 4. a) Schematic representation of the mesoporous silica and allyl silica composite material fabrication procedure: After deposition of the first mesostructured silica thin film, Au/Ag NPs are immobilized on the outer film surface followed by deposition of the second layer and template removal to the final architectures. b) SEM micrograph of a mesoporous silica composite's cross section depicting mainly the top mesoporous layer located on top of the bottom layer and alloy Au/Ag-NPs. c) Absorption spectra of aqueous alloy Au/Ag NP's suspension (black), mesoporous silica composite (cyan), and mesoporous allyl silica composite (orange). Measurements of composite materials were performed in air.

of Au/Ag-NPs becomes accessible due to electrostatic interaction between the positively charged amine groups with the stabilizing citrate groups of the Au/Ag-NPs. Finally, the desired mesoporous architecture is completed, after deposition of the second silica layer followed by template extraction (Figure 4). Besides these architectures, a reference film comprised of a mesoporous silica double layer without Au/Ag-NPs is prepared and used to validate near field induced polymerization. Single mesoporous silica thin films have a thickness of 564 ± 34 nm and 60 vol% porosity, whereas mesoporous allyl silica thin films have a thickness of 585 ± 12 nm and 59 vol% porosity as obtained by ellipsometry measurements and the BEMT (Table S2, Supporting Information). The permselective filter function of the mesoporous double layered films, without and with the incorporation of Au/Ag-NPs, has been investigated via cyclic voltammetry and can be found in Figure S7, Supporting Information. Au/Ag-NPs show a particle size of 23 ± 2 nm as derived from TEM micrographs (Figure S6, Supporting Information) and an absorption maximum at 459 nm. Immobilization of the Au/Ag-NPs has been investigated by UV–vis spectroscopy. Due to the localized plasmons of the Au/Ag-NPs, the final materials show coloration visible by eye (yellow). By comparison of the UV–vis spectrum of the NPs suspension with the spectra observed from mesoporous composites (Figure 4), a controlled and homogeneous immobilization of the NPs can be stated, since no change in shape of the LSPR absorption is observed, thus aggregate formation is not very probable. However, a redshift of the LSPR absorption maximum is observed upon incorporation into mesoporous silica and even a higher shift is observed when incorporated in mesoporous allyl silica with its lower porosity and higher refractive index. This sensitivity of the plasmon resonance conditions on the refractive index of the nanoparticles vicinity makes them not only interesting for light induced reactions, but also attractive for sensing refractive index changes on the nanoscale, for example, induced by polymer functionalization.

Visible light induced iniferter initiated polymerization of DMAEMA in mesoporous composite materials was carried out by using CDTPA within the above described grafting through approach and by applying an energy dosage of 41.4 J cm^{-2}, which corresponds to an irradiation time of 1 h at a power density of 11.5 mW cm^{-2}. Successful polymer functionalization of the composite materials is again indicated by the C=O

vibrational band of DMAEMA at 1728 cm^{-1} in the ATR-IR spectra which appears for both composite materials as shown in **Figure 5**. As the C=O vibrational band can also be observed in the ATR-IR spectra of the reference material, a far field polymerization is assumed. Reducing the energy dose of the irradiation source to 6.9 J cm^{-2}, similar observations can be made for all three materials, whereas the intensity of the C=O band is reduced in all cases compared to the signal intensity after irradiating with 41.4 J cm^{-2}.

Since the energy of the electromagnetic field of surface plasmons is enhanced as compared to the irradiation beam, plasmon induced iniferter initiated polymerization is expected to be locally limited to the plasmon field when using even lower energy dosage below the threshold energy for polymerization. Therefore, polymerization of DMAEMA in mesoporous composites was performed by applying 0.6 J cm^{-2} which corresponds to an irradiation with 1 mW cm^{-2} for 10 min. Comparing the ATR-IR spectra after polymerization, signals at 1728 cm^{-1} corresponding to the C=O vibrational band can only be detected for composite materials bearing Au/Ag-NPs and do not appear in the spectrum of the reference material indicating a successful near field induced iniferter initiated polymerization of DMAEMA in mesoporous films.

As the plasmonic resonance of metal NPs is highly sensitive to the refractive index of their vicinity, as mentioned above, and can be monitored by investigation of the absorption properties of the composite materials before and after polymerization, polymerization can be directly monitored. In **Figure 6**, absorption spectra of the silica composite and the allyl silica composite before and after polymerization with 41.4 J cm^{-2} (far field) as well as the spectra of the allyl silica composite before and after polymerization with 0.6 J cm^{-2} are shown. After polymer functionalization, a redshift of the LSPR band due to an increase of the refractive index of the nanoparticles vicinity are observed additionally supporting the assumption of local near field induced functionalization with respect to the absorption spectra of the allyl silica composite that has been irradiated with the lowest energy dose of 0.6 J cm^{-2}.

Furthermore, TEM micrographs of the composites that have been irradiated with 41.4 J cm^{-2} depicted in Figure 6 do not indicate nanolocal placement of polymer, whereas the micrograph of the allyl silica composite that has been irradiated with 0.6 J cm^{-2} clearly shows the formation of polymer halos with

**ADVANCED
SCIENCE NEWS**

www.advancedsciencenews.com

**ADVANCED
FUNCTIONAL
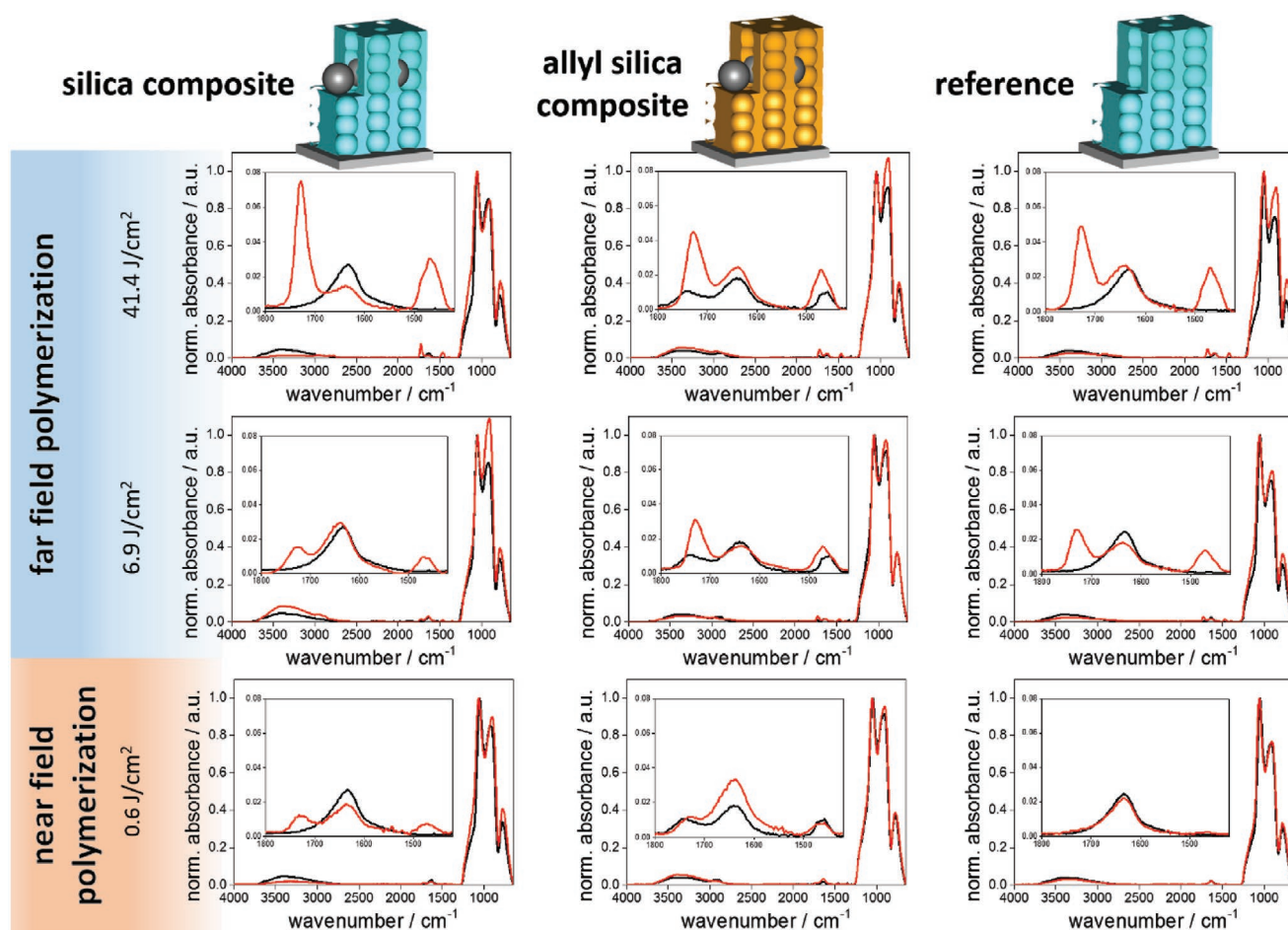MATERIALS**

www.afm-journal.de

Figure 5. ATR-IR spectra of mesoporous silica and allyl silica composites as well as of the reference mesoporous silica double layer (from left to right) before (black curves) and after light induced polymerization of DMAEMA (red curves) by applying an energy dosage of 41.4 J cm^{-2} (top row), 6.9 J cm^{-2} (mid row) and 0.6 J cm^{-2} (bottom row) respectively. For comparison, all spectra are normalized to the Si-O-Si vibrational band at 1050 cm^{-1}.

a thickness of ≈10 nm around the Au/Ag-NPs demonstrating the successful near field induced iniferter initiated polymer functionalization in complex mesoporous architectures on the nanoscale. Further data on near field induced polymerization can be found in Figures S16 and S17, Supporting Information.

3. Conclusion

In summary, two approaches using visible light sensitive iniferter molecules are presented for visible light and surface plasmon induced polymer functionalization of mesoporous silica films in absence of external radical sources or catalysts. Applying SBDTTC, mesoporous silica films were successfully functionalized with PDMAEMA at 430–500 nm in a grafting from approach. Applying CDTPA, mesoporous films were successfully functionalized with PDMAEMA at 473 nm in a grafting through approach. Thereby, PDMAEMA functionalization could be locally limited to the laser spot region. Based on these promising results, PDMAEMA functionalization using iniferter initiated polymerization in a grafting through approach was achieved by surface plasmon irradiation after integrating

plasmonic alloy Ag/Au nanoparticles into mesoporous silica films. We expect this combination of potentially controlled polymerization and nanolocal polymer deposition by using surface plasmons as nanoscale light source for mesoporous film functionalization to open up new pathways for porous hybrid materials and device design.

4. Experimental Section

Materials: Tetraethylorthosilicate (98%, reagent grade) (TEOS), sodium hydride (dry, 95%), carbondisulfide (99.9%),CDTPA (97%), allyltriethoxysilane (AlTES) (96%) and Pluronic F127 were purchased from Sigma Aldrich. (p-Chloromethylphenyl)trimethoxysilane (95%) was received by abcr, Karlsruhe, Germany. Dodecanethiol (98%) was purchased by Alfa Aesar. DMAEMA was purchased from Sigma Aldrich and destabilized over a γ-alumina column prior to use. Anhydrous toluene (0.5 ppm residual water content) and anhydrous tetrahydrofurane (max 0.0075% residual water) were received from AppliChem. All chemicals were used as received unless noted otherwise.

Preparation of Dip Coating Solution for Mesoporous Silica Films: According to reported protocols,[11,44] Pluronic F127 (5.2 g; 0.38 mmol, BioReagent, Sigma Aldrich, 13 800 g mol^{-1}) was suspended in ethanol (48 mL; 820 mmol) under stirring. An aqueous hydrochloric acid solution
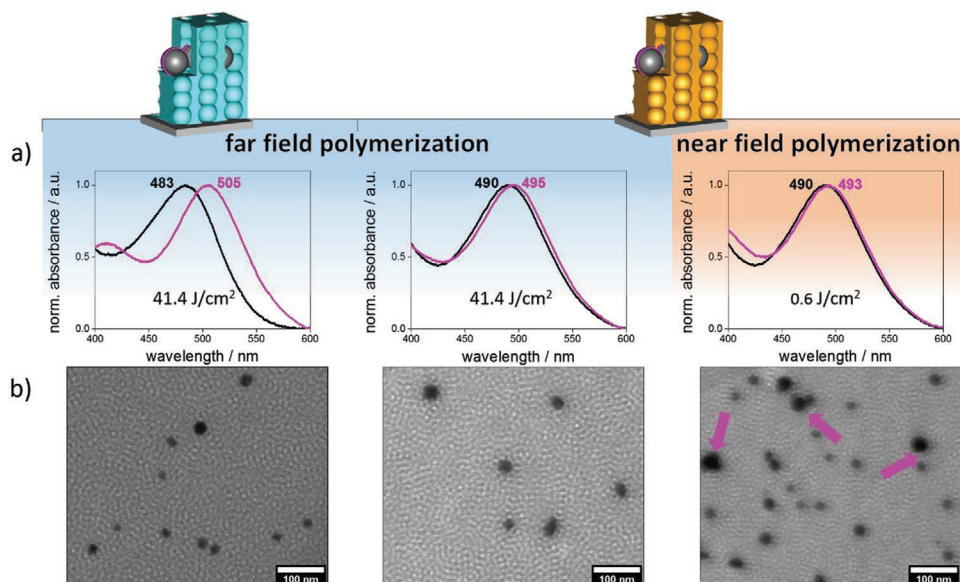
Figure 6. a) Normalized absorption spectra of mesoporous silica composite (left) and mesoporous allyl silica composite (mid) before (black curves) and after far field polymerization of DMAEMA (magenta curves) and of mesoporous allyl silica composite after near field polymerization (right) showing redshifts due to an increase of the refractive index in the vicinity of the NPs. b) TEM micrographs of mesoporous silica composite (left) and mesoporous allyl silica composite (mid) after far field polymerization of DMAEMA and of mesoporous allyl silica composite after near field polymerization (right).

(0.05 mol L^{-1}; 11 mL) was freshly prepared from water (10.44 mL) and hydrochloric acid (37 wt%; 0.66 mL). The acidic solution was added and the template dissolved immediately. TEOS (9.76 mL; 44 mmol) was added and the solution was stirred overnight at room temperature. The molar ratios of the solution were 1 TEOS: 0.009 F127: 19 EtOH: 14 H$_2$O: 0.015 HCl. The solution was stored at −18 °C until being used for mesoporous silica film preparation.

Silica Film Deposition: Glass slides and silicon wafers were cleaned with ethanol and used as substrates for dip coating with a withdrawal speed of 2 mm s^{-1} under controlled environmental conditions (50% rel. humidity, 22–25 °C). Subsequently, the films were stored under these conditions for 60 min followed by a temperature treatment at 60 °C for 60 min, which was followed by a temperature increase to 130 °C within 10 min keeping 130 °C for 60 min. A final heating to 350 °C for 2 h using a heating rate of 1 °C min^{-1} resulted in template calcination.

Synthesis of Alloy Au/Ag-1:1-NPs: Au/Ag-NPs were synthesized based on a reported procedure.[45] A solution of 7.1 mg of HAuCl$_4$·3 H$_2$O (0.018 mmol, 1 eq) in 150 mL of Milli-Q water was refluxed for 10 min. Under vigorous stirring, a solution of 3.1 mg AgNO$_3$ (0.018 mmol, 1 eq) in 170 μL water and a solution of 78.15 mg sodium citrate (0.219 mmol, 24 eq) in 742 μL water were added quickly and the solution was stirred for another 3 h while reducing the temperature to 80 °C. Then, the mixture was cooled to 0 °C and filtered (0.4 μm). The mixture was stored at 4 °C protected from light.

Synthesis of Mesoporous Silica Alloy NP Composite Films: Mesoporous silica thin films were prepared as previously described[46] in accordance via sol-gel chemistry using TEOS and AlTES as inorganic precursors and an amphiphilic triblock copolymer, Pluronic F127, as structure directing template that undergoes micellization upon solvent evaporation resulting in formation of a porous inorganic network. The molar ratios of these compounds in the precursor solution used for dip coating of mesoporous silica thin films were 1 TEOS: 0.009 F127: 19 EtOH: 14 H$_2$O: 0.015 HCl and for dip coating of allyl silica thin films 0.9 TEOS: 0.1 AlTES: 0.01 F127: 19 EtOH: 16.4 H$_2$O: 0.015 HCl resulting in 16 nm mesopores (12 nm pore neck). The precursor solutions were prepared at room temperature and stirred for 20 min before deposition on glass and silicon wafer. The films were dip coated at a withdrawal speed of 2 mm s^{-1} at 23 °C and 50% relative humidity. After deposition, the films were kept at 23 °C and 50% relative humidity for 1 h. The first

film was stabilized by a temperature treatment at 60 and 130 °C for 1 h respectively. For immobilization of Au/Ag-NPs, the mesostructured silica film was functionalized with 3-aminopropyldimethylmethoxysilane using a 0.01 wt% solution in toluene. The reaction mixture as well as the functionalization itself had to be prepared under inert conditions. The reaction mixture was added to the mesostructured film and heated at 80 °C for 1 h. Then, the film was rinsed with toluene and ethanol to remove unbound silane. After drying, the amine functionalized mesostructured film was incubated in the Au/Ag-NP dispersion overnight. The Au/Ag-NP functionalized mesostructured films were then covered with a second silica film via dip coating using the above mentioned conditions and stored at 23 °C and 50% relative humidity for 1 h. Finally, the mesoporous composite material was obtained, after template removal. For silica composites, a consecutive temperature treatment at 60 and 130 °C for 1 h, followed by calcination step up to 350 °C with a heating rate of 1 °C min^{-1} and holding the temperature for 2 h was conducted. In case of co-condensed allyl silica composites, template removal was performed by extracting the mesoporous composite in acidic ethanol (0.01 M HCl) for 3 days after consecutive temperature treatments at 60, 130 °C for 1 h respectively and at 200 °C for 2 h.

Surface Grafting of SBDTTC: Mesoporous silica films deposited on glass substrates or silicon wafers were immersed into a solution of SBDTTC (0.1 M) in toluene. The functionalization was conducted at 70 °C for 4 h. Hereafter, the films were extensively extracted in ethanol for 1 h to remove unbound silane. Prepared films were kept under protection from light until further use.

Surface Initiated Polymerizations with SBDTTC: SBDTTC functionalized mesoporous silica films were placed into a solution of DMAEMA (1.3 mol L^{-1}) in DMSO. The solution was degassed by purging with nitrogen and the sample was irradiated with a lamp (LUMATEC, Superlite S400, Deisenhofen, Germany, Filter 6, 430–500 nm, 12 mW cm^{-2}) for indicated reaction times. Afterward, the substrates were extracted in water for 1 h.

Surface Grafting of Allyl Silane: AlTES (45 μL; 41 mg; 0.2 mmol) was dissolved in toluene (200 mL). Silica films were placed into the silane solution in flame dried flattened schlenk flasks. The samples were heated up to 80 °C for 1 h. The silica films were extensively extracted in ethanol for 1 h to remove unbound silane.

473 nm Laser Induced Polymerizations: Monochromatic and linear, transverse-magnetic polarized (Glan–Thompson polarizer, B. Halle) laser light (Diode pumped solid state laser, Laser 2000, λ = 473 nm, 50 mW) was directed onto the sample placed in the polymerization solution after degassing the solution by purging with nitrogen for 1 min. The polymerization solution was prepared by dissolving CDTPA (46 mg; 0.11 mmol) and DMAEMA (4 mL; 3.7 g; 24 mmol; 1.7 mol L^{-1}) in ethanol (14 mL) with a molar CDTPA to DMAEMA ratio of 1:200. Polymerization was performed at the indicated time and laser beam power. The laser power of the polymerization was controlled by adjusting the angle of the first passed polarizer, according to a two polarizer system described by Malus' law. The laser power versus polarizer angle dependence was determined with a THORLABS PM100A Optical Power Meter after passing two polarizers.

LSPR Induced Polymerization: Polymer functionalization of mesoporous composite materials was performed by mixing 2.9 g (18 mmol) destabilized DMAEMA and 40 mg CDTPA (99 µmol) in 10 mL absolute ethanol. The solution was purged with nitrogen for 10 min and then transferred to cuvettes in which the mesoporous composite material was placed. The cuvettes were irradiated with a lamp (LUMATEC, Superlite S400, Deisenhofen, Germany, Filter 6, 430–500 nm) using a power density of 1 mW cm^{-2} for 10 min and 11.5 mW cm^{-2} for 1 h at a distance of 10 cm to the irradiation source. Subsequently, the substrates were extracted with ethanol for 30 min before drying and storing under ambient conditions.

Infrared Spectroscopy: IR spectra were recorded in ATR mode using a Spectrum One FT-IR spectrometer from Perkin–Elmer. Corresponding spectra were recorded directly from the substrate or from films, which were scratched off the substrate. Each spectrum was recorded from 4000 to 650 cm^{-1}. The spectra were background corrected and normalized to the Si-O-Si asymmetric stretching vibrational band at 1050 cm^{-1}.

CO_2-Plasma Treatment: CO_2-plasma treatment was performed according to a literature protocol[7b,40] using a Femto SRS plasma generator (Diener electronics, model Femto, 13.56 MHz, maximum RF power: 200 W). The samples were degassed and CO_2 gas was introduced. The RF generator was switched on for 12 s after a stable pressure of 0.3 mbar was achieved.

Thermogravimetric Analysis: TGA was recorded in a Mettler–Toledo instrument (TGA 1) recorded in air atmosphere. The samples obtained by scratching off the mesoporous silica films from its glass supports were heated from room temperature to a final temperature of 600 °C with a heating rate of 10 K min^{-1}.

UV–Vis Spectroscopy: UV–vis spectra were recorded with an Agilent Cary 60 UV–vis spectrometer. All spectra were background corrected to the respective solvent.

Supporting Information

Supporting Information is available from the Wiley Online Library or from the author.

Acknowledgements

Conflict of Interest

The authors declare no conflict of interest.

Data Availability Statement

Research data are not shared.

[1] a) C. Ghazaly, M. Hébrant, E. Langlois, B. Castel, M. Guillemot, M. Etienne, *Sensors* **2019**, *19*, 3508; b) A. Mutschler, V. Stock, L. Ebert, E. M. Björk, K. Leopold, M. Lindén, *Nanomaterials* **2019**, *9*, 35; c) M. Saadaoui, I. Fernández, G. Luna, P. Diez, S. Campuzano, N. Raouafi, A. Sánchez, J. M. Pingarrón, R. Villalonga, *Anal. Bioanal. Chem.* **2016**, *408*, 7321.

[2] N. Vilà, E. André, R. Ciganda, J. Ruiz, D. Astruc, A. Walcarius, *Chem. Mater.* **2016**, *28*, 2511.

[3] a) M. Rafti, A. Brunsen, M. C. Fuertes, O. Azzaroni, G. J. Soler-Illia, *ACS Appl. Mater. Interfaces* **2013**, *5*, 8833; b) P.-H. Wu, P. Mäkie, M. Odén, E. M. Björk, *Nanomaterials* **2019**, *9*, 562;

[4] A. Calvo, B. Yameen, F. J. Williams, G. J. A. A. Soler-Illia, O. Azzaroni, *J. Am. Chem. Soc.* **2009**, *131*, 10866.

[5] S. Schmidt, S. Alberti, P. Vana, G. J. A. A. Soler-Illia, O. Azzaroni, *Chem. - Eur. J.* **2017**, *23*, 14500.

[6] L. Silies, A. Andrieu-Brunsen, *Langmuir* **2017**, *34*, 807.

[7] a) A. K. Bohaty, M. R. Newton, I. Zharov, *J. Porous Mater.* **2010**, *17*, 465; b) F. Krohm, J. Kind, R. Savka, M. A. Janßen, D. Herold, H. Plenio, C. M. Thiele, A. Andrieu-Brunsen, *J. Mater. Chem. C* **2016**, *4*, 4067.

[8] a) Z. S. Siwy, S. Howorka, *Chem. Soc. Rev.* **2010**, *39*, 1115; b) S. F. Buchsbaum, G. Nguyen, S. Howorka, Z. S. Siwy, *J. Am. Chem. Soc.* **2014**, *136*, 9902; c) J. Elbert, F. Krohm, C. Rüttiger, S. Kienle, H. Didzoleit, B. N. Balzer, T. Hugel, B. Stühn, M. Gallei, A. Brunsen, *Adv. Funct. Mater.* **2014**, *24*, 1591.

[9] a) M. Kruk, *Isr. J. Chem.* **2012**, *52*, 246; b) A. Gamero-Quijano, C. Karman, N. Vilà, G. g. Herzog, A. Walcarius, *Langmuir* **2017**, *33*, 4224; c) A. Andrieu-Brunsen, S. Micoureau, M. Tagliazucchi, I. Szleifer, O. Azzaroni, G. J. A. A. Soler-Illia, *Chem. Mater.* **2015**, *27*, 808; d) L. Silies, H. Didzoleit, C. Hess, B. Stühn, A. Andrieu-Brunsen, *Chem. Mater.* **2015**, *27*, 1971.

[10] a) J. C. Tom, R. Brilmayer, J. Schmidt, A. Andrieu-Brunsen, *Polymers* **2017**, *9*, 539; b) R. Brilmayer, C. Hess, A. Andrieu-Brunsen, *Small* **2019**, *15*, 1902710.

[11] R. Brilmayer, S. Kübelbeck, A. Khalil, M. Brodrecht, U. Kunz, H. J. Kleebe, G. Buntkowsky, G. Baier, A. Andrieu-Brunsen, *Adv. Mater. Interfaces* **2020**, *7*, 1901914.

[12] A. M. M. Jani, I. M. Kempson, D. Losic, N. H. Voelcker, *Angew. Chem., Int. Ed.* **2010**, *49*, 7933.

**ADVANCED
SCIENCE NEWS**

www.advancedsciencenews.com

**ADVANCED
FUNCTIONAL
MATERIALS**

www.afm-journal.de

[13] M. Ochs, R. Mohammadi, N. Vogel, A. Andrieu-Brunsen, *Small* **2020**, *16*, 1906463.

[14] a) C. Deeb, C. Ecoffet, R. Bachelot, J. Plain, A. Bouhelier, O. Soppera, *J. Am. Chem. Soc.* **2011**, *133*, 10535; b) T. Ding, J. Mertens, A. Lombardi, O. A. Scherman, J. J. Baumberg, *ACS Photonics* **2017**, *4*, 1453; c) H. Minamimoto, T. Toda, R. Futashima, X. Li, K. Suzuki, S. Yasuda, K. Murakoshi, *J. Phys. Chem. C* **2016**, *120*, 16051; d) Y. Takahashi, Y. Furukawa, T. Ishida, S. Yamada, *Nanoscale* **2016**, *8*, 8520; e) Y. Wang, S. Wang, S. Zhang, O. A. Scherman, J. J. Baumberg, T. Ding, H. Xu, *Nano Res.* **2018**, *11*, 6384; f) K.-H. Dostert, M. Álvarez, K. Koynov, A. n. del Campo, H.-J. r. Butt, M. Kreiter, *Langmuir* **2012**, *28*, 3699.

[15] G. Cortial, M. Siutkowski, F. Goettmann, A. Moores, C. Boissière, D. Grosso, P. Le Floch, C. Sanchez, *Small* **2006**, *2*, 1042.

[16] a) L. Bois, F. Chassagneux, Y. Battie, F. Bessueille, L. Mollet, S. Parola, N. Destouches, N. Toulhoat, N. Moncoffre, *Langmuir* **2010**, *26*, 1199; b) C. M. Leroy, T. Cardinal, V. Jubera, C. Aymonier, M. Treguer-Delapierre, C. Boissière, D. Grosso, C. Sanchez, B. Viana, F. Pellé, *Microporous Mesoporous Mater.* **2013**, *170*, 123.

[17] a) P. C. Angelomé, L. M. Liz-Marzán, *J. Phys. Chem. C* **2010**, *114*, 18379; b) M. M. Zalduendo, V. Oestreicher, J. Langer, L. M. Liz-Marzán, P. C. Angelomé, *Anal. Chem.* **2020**, *92*, 13656.

[18] P. C. Angelomé, L. M. Liz-Marzán, *J. Sol-Gel Sci. Technol.* **2014**, *70*, 180.

[19] P. C. Angelomé, I. Pastoriza-Santos, J. Pérez-Juste, B. Rodríguez-González, A. Zelcer, G. J. A. A. Soler-Illia, L. M. Liz-Marzán, *Nanoscale* **2012**, *4*, 931.

[20] a) K. L. Kelly, E. Coronado, L. L. Zhao, G. C. Schatz, *J. Phys. Chem. B* **2003**, *107*, 668; b) K.-S. Lee, M. A. El-Sayed, *J. Phys. Chem. B* **2006**, *110*, 19220; c) M. A. Garcia, *J. Phys. D: Appl. Phys.* **2012**, *45*, 389501.

[21] a) G. J. A. A. Soler-Illia, O. Azzaroni, *Chem. Soc. Rev.* **2011**, *40*, 1107; b) P. Innocenzi, L. Malfatti, *Chem. Soc. Rev.* **2013**, *42*, 4198; c) S. Alberti, G. J. A. A. Soler-Illia, O. Azzaroni, *Chem. Commun.* **2015**, *51*, 6050; d) Z. Zhang, L. Wen, L. Jiang, *Chem. Soc. Rev.* **2018**, *47*, 322; e) M. Tiemann, C. Weinberger, *Adv. Mater. Interfaces* **2020**, *8*, 2001153.

[22] a) B. P. Fors, C. J. Hawker, *Angew. Chem., Int. Ed.* **2012**, *51*, 8850; b) N. J. Treat, B. P. Fors, J. W. Kramer, M. Christianson, C.-Y. Chiu, J. Read de Alaniz, C. J. Hawker, *ACS Macro Lett.* **2014**, *3*, 580.

[23] a) A. J. Boydston, K. A. Ogawa, A. E. Goetz, *Synlett* **2015**, *27*, 203; b) P. Lu, N. M. Alrashdi, A. J. Boydston, *J. Polym. Sci., Part A: Polym. Chem.* **2017**, *55*, 2977.

[24] N. Herzog, J. Kind, C. Hess, A. Andrieu-Brunsen, *Chem. Commun.* **2015**, *51*, 11697.

[25] a) T. G. McKenzie, Q. Fu, E. H. H. Wong, D. E. Dunstan, G. G. Qiao, *Macromolecules* **2015**, *48*, 3864; b) J. Yeow, O. R. Sugita, C. Boyer, *ACS Macro Lett.* **2016**, *5*, 558.

[26] X. Liu, Y. Ni, J. Wu, H. Jiang, Z. Zhang, L. Zhang, Z. Cheng, X. Zhu, *Polym. Chem.* **2018**, *9*, 584.

[27] C. Aydogan, G. Yilmaz, Y. Yagci, *Macromolecules* **2017**, *50*, 9115.

[28] A. Bagheri, J. Yeow, H. Arandiyan, J. Xu, C. Boyer, M. Lim, *Macromol. Rapid Commun.* **2016**, *37*, 905.

[29] J.-P. Fouassier, F. Morlet-Savary, J. Lalevée, X. Allonas, C. Ley, *Materials* **2010**, *3*, 5130.

[30] M. Erzina, O. Guselnikova, P. Postnikov, R. Elashnikov, Z. Kolska, E. Miliutina, V. Švorčík, O. Lyutakov, *Adv. Mater. Interfaces* **2018**, *5*, 1801042.

[31] J. Jiang, G. Ye, F. Lorandi, Z. Liu, Y. Liu, T. Hu, J. Chen, Y. Lu, K. Matyjaszewski, *Angew. Chem.* **2019**, *131*, 12224.

[32] N. Corrigan, D. Rosli, J. W. J. Jones, J. Xu, C. Boyer, *Macromolecules* **2016**, *49*, 6779.

[33] J. Yeow, R. Chapman, J. Xu, C. Boyer, *Polym. Chem.* **2017**, *8*, 5012.

[34] C. A. Figg, J. D. Hickman, G. M. Scheutz, S. Shanmugam, R. N. Carmean, B. S. Tucker, C. Boyer, B. S. Sumerlin, *Macromolecules* **2018**, *51*, 1370.

[35] M. Li, M. Fromel, D. Ranaweera, S. Rocha, C. Boyer, C. W. Pester, *ACS Macro Lett.* **2019**, *8*, 374.

[36] F. Kameche, W. Heni, S. Telitel, D. Ge, L. Vidal, F. Dumur, D. Gigmes, J. Lalevée, S. Marguet, L. Douillard, C. Fiorini-Debuisschert, R. Bachelot, O. Soppera, *Mater. Today* **2020**, *40*, 38.

[37] T. Otsu, M. Yoshida, T. Tazaki, *Makromol. Chem., Rapid Commun.* **1982**, *3*, 133.

[38] a) M. J. Garcia-Soto, K. Haupt, C. Gonzato, *Polym. Chem.* **2017**, *8*, 4830; b) Z. Huang, T. Qiu, H. Xu, H. Shi, J. Rui, X. Li, L. Guo, *Macromolecules* **2018**, *51*, 7329; c) M. Rubens, P. Latsrisaeng, T. Junkers, *Polym. Chem.* **2017**, *8*, 6496; d) S. Shanmugam, J. Cuthbert, J. Flum, M. Fantin, C. Boyer, T. Kowalewski, K. Matyjaszewski, *Polym. Chem.* **2019**, *10*, 2477.

[39] a) C. Boissiere, D. Grosso, S. Lepoutre, L. Nicole, A. B. Bruneau, C. Sanchez, *Langmuir* **2005**, *21*, 12362; b) J. E. Spanier, I. P. Herman, *Phys. Rev. B: Condens. Matter Mater. Phys.* **2000**, *61*, 10437.

[40] D. J. Babu, S. Yadav, T. Heinlein, G. Cherkashinin, J. J. Schneider, *J. Phys. Chem. C* **2014**, *118*, 12028.

[41] a) M. Save, G. Granvorka, J. Bernard, B. Charleux, C. Boissière, D. Grosso, C. Sanchez, *Macromol. Rapid Commun.* **2006**, *27*, 393; b) H. Naono, R. Fujiwara, M. Yagi, *J. Colloid Interface Sci.* **1980**, *76*, 74.

[42] a) H. Hemmatpour, V. Haddadi-Asl, H. Roghani-Mamaqani, *Polymer* **2015**, *65*, 143; b) J. M. Cervantes-Uc, J. V. Cauich-Rodríguez, W. A. Herrera-Kao, H. Vázquez-Torres, A. Marcos-Fernández, *Polym. Degrad. Stab.* **2008**, *93*, 1891.

[43] C. J. Brinker, Y. Lu, A. Sellinger, H. Fan, *Adv. Mater.* **1999**, *11*, 579.

[44] D. R. Dunphy, P. H. Sheth, F. L. Garcia, C. J. Brinker, *Chem. Mater.* **2015**, *27*, 75.

[45] M. Roskamp, *Oberflächenfunktionalisierung von Nanopartikeln zur gezielten Wechselwirkung mit Biomolekülen*, Freie Universität Berlin **2010**.

[46] N. Herzog, R. Brilmayer, M. Stanzel, A. Kalyta, D. Spiehl, E. Dörsam, C. Hess, A. Andrieu-Brunsen, *RSC Adv.* **2019**, *9*, 23570.

2009732 (9 of 9)